Journal of the Optical Society of America B
OPTICAL PHYSICS

Observation of whispering gallery modes in elastic light scattering from microdroplets optically trapped in a microfluidic channel

S. Anand,[1] M. Eryürek,[1] Y. Karadag,[2] A. Erten,[1] A. Serpengüzel,[1] A. Jonáš,[3] and A. Kiraz[1,4,*]

[1]Department of Physics, Koç University, Sariyer, Istanbul 34450, Turkey
[2]Department of Physics, Marmara University, Göztepe, Istanbul 34722, Turkey
[3]Department of Physics, Istanbul Technical University, Maslak, Istanbul 34469, Turkey
[4]Department of Electrical and Electronics Engineering, Koç University, Sariyer, Istanbul 34450, Turkey
*Corresponding author: akiraz@ku.edu.tr

Received 10 May 2016; accepted 11 May 2016; posted 13 May 2016 (Doc. ID 264968); published 6 June 2016

Optical whispering gallery modes (WGMs) were observed in elastic scattering spectra recorded from oil-in-water emulsion droplets in a microfluidic channel. Droplets with diameters ranging between 15 and 50 μm were trapped by optical tweezers near the tip of a single mode fiber that enabled the excitation of the WGMs using a tunable laser. Quality factors of the WGMs were observed to increase with droplet size. WGMs with quality factors of more than 10^4 were observed for droplets with diameters around 45 μm. In some cases, recorded WGMs drifted monotonically to the blue end of the spectrum due to droplet dissolution in the host liquid. Fluctuating spectral shifts to both blue and red ends of the spectrum were also observed. These were attributed to the presence of randomly diffusing particulate contaminants in the droplet liquid, indicating the potential of optically trapped droplet resonators for optical sensing applications.

OCIS codes: (290.0290) Scattering; (140.3945) Microcavities; (350.4855) Optical tweezers or optical manipulation; (280.4788) Optical sensing and sensors; (060.2310) Fiber optics; (300.6360) Spectroscopy, laser.

http://dx.doi.org/10.1364/JOSAB.33.001349

1. INTRODUCTION

Light in a spherical microcavity with a refractive index higher than that of the surrounding medium can be confined by total internal reflections at the interface between the microsphere and the surrounding medium. Consequently, electromagnetic waves coupled into the cavity or emitted from a gain medium inside the cavity meeting the requirements for constructive interference form cavity resonances called whispering gallery modes (WGMs) [1–3]. The energy stored in the cavity at resonant frequencies increases due to large quality factors (Q-factors) of these resonances granted by the highly symmetric spherical geometry of the cavity. The combination of high Q-factors and microscale mode volumes makes microsphere resonators unique for studying cavity lasing in solid [4,5] or liquid phase [6], and allows lasing operation with a very low pump threshold [7]. Narrow resonance linewidths resulting from the high Q-factors inspire applications in channel filtering [8,9]. Also, the sensitivity of sharp WGM resonances to small changes in temperature and refractive index or to the presence of contamination makes them one of the most sensitive probes for biological or chemical sensing applications [10].

Droplet-based resonators, the fluidic equivalent of solid spherical resonators, are among the oldest WGM cavities, first studied more than 30 years ago [2] and shown to exhibit ultrahigh Q-factors [11]. Due to their tendency to minimize the interfacial energy by minimizing surface area, liquid droplets of the 1–100 μm size range (smaller than the capillary length of the droplet liquid) are almost ideal spherical particles with surface roughness typically of the order of a few Ångström, which reduces the scattering loss of cavity photons and increases the Q-factor [12]. Besides, by a suitable choice of operating wavelength, light absorption by the droplet material can be avoided to further reduce the optical loss at the wavelength of the cavity-supported WGMs.

Introduction of optical tweezers for immobilizing individual dielectric microparticles by a tightly focused laser beam can greatly simplify precise light-scattering measurements with such particles [13,14]. With optical trapping, studied particles are held away from interfering obstacles so that they can be observed for long time [2]. Micrometer-sized liquid droplets can be easily produced using aerosol generators in air or as emulsions by simple mechanical agitation and subsequently introduced into an optical trap. In this article, we report

resonantly enhanced elastic light scattering from WGMs of individual liquid droplets optically trapped in an immiscible liquid inside a microfluidic channel. Droplet WGMs are excited by free-space coupling of light to the trapped droplet with a single-mode optical fiber. For different cases, we show either a steady spectral drift of WGMs to the blue end of the spectrum or fluctuating spectral shifts to both blue and red ends of the spectrum, attributed to the droplet dissolution and the presence of diffusing particulate contaminants in the droplet liquid, respectively. We also study the dependence of the measured Q-factors on the size of the cavity and demonstrate smaller Q-factors with decreasing droplet size as a result of higher radiative losses.

Chemical and biological detection based on Q-factor change has been shown before with solid microcavities [15,16]. In a recent report, Q-factor change was used as a contamination detector for relatively large liquid droplets with diameters of 0.5–1.5 mm suspended in air from the tip of a needle [17]. In contrast to this work where free-space coupling was used to observe WGMs of millimetric oil droplets suspended in air, our droplets are comparatively small (diameters ranging between 12 and 54 μm), immersed in deionized (DI) water, and controlled by optical tweezers within a microfluidic channel. Recently, optical tweezing was also used to achieve optical coupling between emulsion microdroplets of paraffin oil in DI water and tapered optical fiber waveguides in order to record droplet WGM spectra [18]. However, fluctuations of WGM spectral positions were not studied for extended times in this recent work. Besides, our experimental geometry is simpler, more robust, and better suited for microfluidic integration because it does not require the use of a tapered optical fiber.

2. EXPERIMENTAL SETUP AND PROCEDURES

The experimental setup shown in Fig. 1 was used for WGM spectroscopy of individual optically trapped emulsion droplets. Emulsions used in our study consisted of microdroplets of benzyl benzoate (BB) (refractive index [RI] = 1.568 at $\lambda = 589$ nm, $\rho = 1.11$ g/cm^3 at 20°C, viscosity 8.29 cP at 25°C) dispersed in DI water (RI = 1.334 at $\lambda = 589$ nm, $\rho = 1.00$ g/cm^3 at 20°C) mixed with 1% sodium dodecyl sulfate. The saturation concentration and diffusion coefficient of BB in water are 0.015 kg/m^3 and 0.539×10^{-9} m^2/s, respectively. BB was selected for our studies because of its relatively high refractive index and slightly higher density than DI water that enables easy optical trapping using an inverted geometry. Emulsions of BB in water were prepared by manual agitation of a mixture of BB and water and subsequently introduced into a polydimethylsiloxane (PDMS) microfluidic chip featuring a single channel of 160 μm width. The chip supported a single-mode optical fiber (cleaved at 90° with respect to the fiber axis) of 125 μm outer diameter with core diameter of 8 μm, placed orthogonal to the walls of the channel. The channel had one inlet connected with a syringe via flexible tubing to inject emulsions and one outlet for washing solutions. A continuous wave (CW) 1070 nm ytterbium fiber laser with 10 W maximum output power was used to create an independent single beam optical trap. This laser beam was sent through a 3× beam expander and reflected from a dichroic mirror (D1) before being focused into the channel by a water-immersion microscope objective (NA = 1.2, 60×) in the inverted geometry.

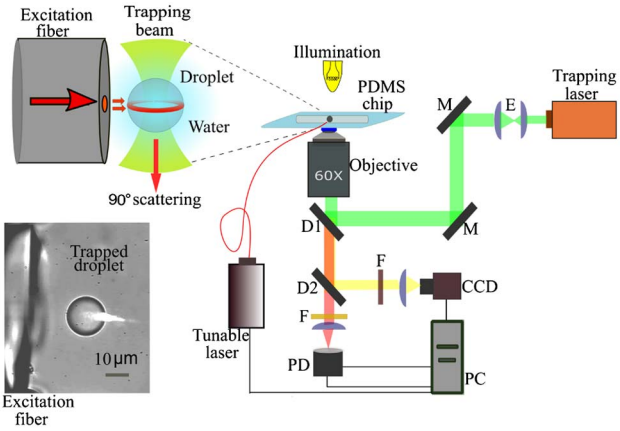

Fig. 1. Sketch of the experimental setup used for microdroplet scattering experiments. The inset shows an image of scattered light (glare spot) when an optically trapped droplet was excited by a red laser. D1, D2: dichroic mirrors, F: IR filters, M: mirrors, PD: photodetector, E: beam expander.

The objective lens that was used for imaging, three-dimensional optical manipulation, and collection of light scattered from the trapped droplet was attached to a manual XYZ stage that allowed for positioning of the lens with respect to the sample chamber. The trapped droplet was held tightly within the channel inside the PDMS chip which was mounted on another piezo-driven 3D positioning stage. This fine-positioning stage was extremely helpful in achieving optimal coupling of tunable laser light into the droplet through fine adjustment of the fiber tip (up to 100 μm in nanometer steps) in all three directions. The whole experimental procedure was fairly quick: once a droplet was trapped near the fiber tip, within several minutes coupling was achieved for light scattering experiments. When needed, the trap position within the sample chamber could be further controlled by changing the separation distance between the expander lenses and steering them in the direction perpendicular to the beam axis. Using this setup, BB droplets of diameters up to ~45 μm could be stably trapped. The typical power used to trap the droplets was 200–300 mW at the sample plane. BB droplets of diameters 45–55 μm were harder to trap due to their comparatively large size. However, by optimizing the trapping power and the distance between the two expander lenses, we overcame this issue. Visible light in the imaging path of the setup was diverted to an ordinary CCD camera via a dichroic mirror (D2). Excitation of WGMs of the studied microdroplet was achieved using a CW, tunable infrared (IR) laser (tuning range: 1500–1630 nm; wavelength resolution: 1 pm) that was coupled to the single mode optical fiber suspended in the chip. For visualization purposes, we also used a red laser ($\lambda = 638$ nm), coupled to the same optical fiber, that allowed for the observation of resonant light scattering from the droplet in recorded images (see inset of Fig. 1). In WGM spectroscopic measurements, while the IR laser wavelength was swept over the range of interest, intensity of light scattered from the droplet was collected by the microscope

objective in the direction perpendicular to the excitation of the droplet, and subsequently relayed to an InGaAs photodetector (PD). The PD signal was amplified by a current amplifier and digitized using a custom-written computer code. Peaks corresponding to different WGMs were observed when the PD signal was plotted as a function of the excitation laser wavelength, as shown in Fig. 2. Q-factors of WGMs were calculated from the full width at half-maximum (FWHM) of Lorentzian fits to the recorded peaks using $Q = \lambda_0/\Delta\lambda_0$, where λ_0 and $\Delta\lambda_0$ indicate the WGM central wavelength and FWHM in vacuum, respectively.

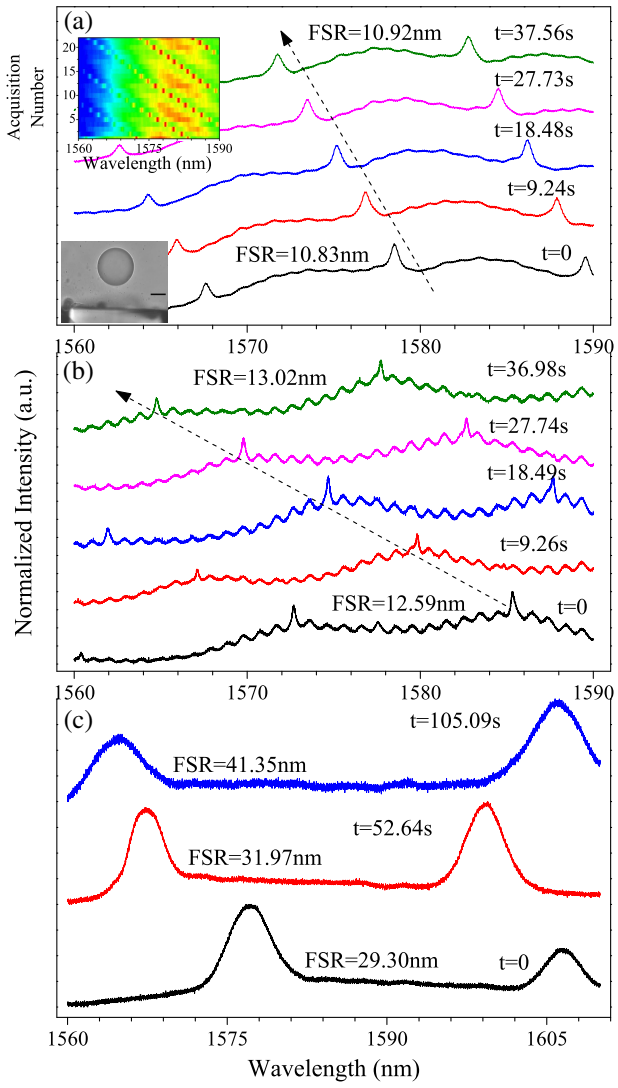

Fig. 2. Measured scattering spectra of BB droplets of initial diameters around (a) 49 μm, (b) 42 μm, and (c) 18 μm, optically trapped in water. The spectra were recorded in bottom-to-top order at time intervals indicated by the labels. The spectra have been offset vertically for clarity. Temporal evolution of 28 consecutive spectra recorded from the same droplet is shown in the inset of (a) as a 2D spectral plot (horizontal axis: wavelength; vertical axis: acquisition number; color coding: red—high intensity, blue—low intensity). Another inset in (a) shows the image of the studied droplet; scale bar is 20 μm.

3. EXPERIMENTAL LIMITS ON Q-FACTOR MEASUREMENTS

The overall Q-factor of the cavity WGMs is given by

$$Q^{-1} = Q_{\text{mat}}^{-1} + Q_{\text{s.s.}}^{-1} + Q_{\text{rad}}^{-1}, \tag{1}$$

determined by the absorptive Q_{mat}^{-1}, surface scattering $Q_{\text{s.s.}}^{-1}$, and radiative Q_{rad}^{-1} losses in the resonator. Absorptive and surface-scattering losses are given as

$$Q_{\text{mat}} = \frac{2\pi n_{\text{int}}}{\alpha\lambda_0} \tag{2}$$

and

$$Q_{\text{s.s.}} = \frac{\lambda_0^2 d}{2\pi^2\sigma^2 B n_{\text{ext}}^2}, \tag{3}$$

where n_{int} and α are the droplet refractive index and absorption coefficient, n_{ext} is the refractive index of the host medium, d is the droplet diameter, and σ and B are the rms size and the correlation length of surface inhomogeneities [19,20]. Thermal excitation of droplets results in random dynamic distortions of the droplet shape with a characteristic amplitude σ that reads as [21]

$$\sigma = \left[\frac{k_B T}{4\pi\gamma}\right]^{1/2}, \tag{4}$$

where k_B is the Boltzmann constant, T is the thermodynamic temperature, and γ is the droplet interfacial tension. Aas *et al.* [22] measured the interfacial tension of microscopy immersion oil in contact with water, a liquid–liquid system similar to the emulsions of BB in water used in this work. They found the value of $\gamma = 13.1$ mN/m for the interface between pure immersion oil and water; this value dropped down to approximately 1.5 mN/m in the presence of a surfactant. Assuming the average value of $\gamma \approx 7$ mN/m at the room temperature $T = 293$ K, rms surface roughness $\sigma \approx 0.2$ nm. The correlation length of surface inhomogeneities B can be estimated from the characteristic wavenumber q of the maximal liquid surface roughness ($q \sim 10^7$ cm^{-1}) as $B \approx 2\pi/q \approx 6.3$ nm [23]. For a droplet of diameter $d = 42$ μm studied at the mean resonant wavelength $\lambda_0 = 1575$ nm, Eq. (3) then gives $Q_{\text{s.s.}} \approx 1.2 \times 10^{10}$, significantly higher than our experimentally observed Q-factors. Therefore, we can rule out surface scattering due to thermal excitation as the main constraint setting the overall Q-factor in our measurements. However, as we discuss later, surface scattering due to large contaminant particles can still limit the observed Q-factors in our experiments.

Radiative loss is given by [24]

$$Q_{\text{rad}} = x \exp\left[2\nu g\left(\frac{x}{\nu}\right)\right], \tag{5}$$

where $g(y) = -\sqrt{1-y^2} + \arg\cosh(1/y)$, $x = \pi d n_{\text{ext}}/\lambda_0$ is the size parameter, $\nu = l + 1/2$, and l is the angular momentum number corresponding to the number of wavelengths in the circumference of droplet ($l \simeq \pi d n_{\text{int}}/\lambda_0$) [25,26].

The free spectral range (FSR) can be determined directly from the mode spectra. The diameters of the trapped oil droplets were calculated from the WGM FSR in vacuum (FSR_0), mean scattering wavelength λ_0, and known RIs of the droplet

($n_{int} = 1.568$) and host liquid (water, $n_{ext} = 1.334$) liquids, using an asymptotic formula of Chýlek *et al.* [27]:

$$d = \frac{\lambda_0^2}{\pi n_{ext} \mathrm{FSR}_0} \frac{\arctan([(n_{int}/n_{ext})^2 - 1]^{1/2})}{[(n_{int}/n_{ext})^2 - 1]^{1/2}}. \quad (6)$$

4. RESULTS AND DISCUSSION

The emulsion system used in our study consisted of virtually immiscible liquids, which provided a good RI contrast and a small density difference between the droplet and the surrounding medium. This implies a strong confinement of WGMs inside the trapped microdroplet together with stable optical trapping that is not strongly affected by buoyancy.

When the tunable IR laser beam was coupled efficiently to the rim of the droplet, WGMs were observed as peaks in the scattering spectra. Figure 2 shows scattering spectra recorded from exemplary BB droplets of three different sizes at room temperature (22.7°C). For all three droplets, a pattern of WGMs separated by FSR is clearly visible. The acquisition time of each spectrum was ~9.25 s. For the droplets shown in Figs. 2(a) and 2(b), the wavelength was scanned over a spectral range of 30 nm, and high-Q WGMs were excited after optimizing the coupling through fine 3D positioning and stabilization of the droplet. Since a polarization-maintaining fiber was not used in the experiments, TE- and TM-polarized WGMs could not be excited in a selective manner. This prevented us from exact identification of the observed WGMs. However, good match between experimentally recorded FSRs and their expected values calculated from the droplet sizes and RIs of the droplet and host liquid verifies that the spectral features observed in the scattering spectra are indeed WGMs, which was the most relevant information in our experiments.

During subsequent spectral scans, positions of individual WGMs typically displayed blue spectral shift, indicating partial dissolution of BB droplets in water. The observed dissolution of freshly prepared droplet was faster [blueshift of 20.6 nm within 37 s shown in Fig. 2(b)] in comparison to droplet stored for two days [blueshift of 6.8 nm within 38 s shown in Fig. 2(a)]. This change in the dissolution rates of the droplets was attributed to the saturation of BB solution in DI water over time. In general, droplet dissolution rate is a function of ambient temperature, which in turn depends on the used power of the trapping laser. In this context, we note that time $t = 0$ shown in Fig. 2 does not indicate the time instant when the trapping laser was activated. The droplets were typically trapped for several minutes and their positions were optimized before starting with spectral recordings. Hence, any increase in the droplet temperature induced by trapping laser heating is expected to reach a steady state before the scattering spectra are recorded. For a typical laser power of 200–300 mW at the sample and droplets of diameter 20–50 μm trapped by 1064 nm light at a distance of 10 μm from the cover slip, the droplet temperature increase is estimated to be 2–4 K [28], that is, not too dramatic. Different dissolution rates observed in Figs. 2(a) and 2(b) under similar trapping laser powers for droplets of comparable sizes also indicate that the observed change in dissolution rates is due to saturation of the solution rather than heating by the trapping laser.

As discussed by Aas *et al.* [22] the increase in droplet temperature leads to a change in oil and water RIs by $\Delta n_{int}/(n_{int}\Delta T) \sim -2 \times 10^{-4}$ K^{-1} and $\Delta n_{ext}/(n_{ext}\Delta T) \sim -1 \times 10^{-4}$ K^{-1}, respectively. These give an uncertainty in droplet size determination using Eq. (6). For our case, for a maximum temperature increase of 4 K, this uncertainty in droplet diameter is estimated to be less than ±0.02 μm.

In all experimental runs, the observed WGMs were superimposed on an oscillating spectral background [see Fig. 2(b) for illustration]. In contrast to the droplet WGMs, the spectral positions of these background ripples remained constant during subsequent spectral scans, and their separation ($\Delta\lambda \sim 1$ nm) was significantly smaller than the droplet FSR. We attribute these ripples to light interference taking place in glass components used in the detection path of our experimental setup. Plan–parallel optical elements of thickness l and RI n_g can be represented as Fabry–Perot cavities with mode spacing $\Delta\lambda$ at the mean light wavelength λ_0 given by

$$\Delta\lambda = \frac{\lambda_0^2}{2 n_g l \cos\theta}, \quad (7)$$

where θ is the angle between the light propagation direction and the surface normal of the element. Using our experimental data ($\lambda_0 = 1550$ nm, $\Delta\lambda = 1$ nm, RI of glass $n_g = 1.5$), the thickness l of the element causing the interference effects should be ~0.8 mm (assuming $\theta = 0°$). This is quite close to ~1 mm, which is the typical thickness of the optical filters and dichroic mirrors used in the setup. From the drawing of the experimental setup (Fig. 1), we suspect that the interference arises in dichroic mirrors D1, D2 or in the filter placed just in front of the PD.

Further insight into the droplet dissolution dynamics can be gained by analyzing the temporal evolution of the droplet FSR, which reveals the droplet diameter d through the asymptotic formula (6). Figure 2(a) shows a nominal FSR increase from 10.83 nm [corresponding to $d = (48.70 \pm 0.02)$ μm] to 10.92 nm [corresponding to $d = (48.30 \pm 0.02)$ μm] after a time span of 37.6 s, indicating the droplet size is quite stable compared to the case of fresh droplets. This is also illustrated by the color plot of consecutive scattering spectra shown in the inset of Fig. 2(a). On the other hand, for a freshly prepared droplet shown in Fig. 2(b), the FSR increases more significantly—from 12.59 nm [$d = (41.90 \pm 0.02)$ μm] to 13.02 nm [$d = (40.50 \pm 0.02)$ μm] within 37.0 s—due to dissolution of the droplet into the carrier fluid. The initial size of the droplet studied in Fig. 2(a) determined from image analysis is 49 μm, showing a very good agreement with the values obtained from Eq. (6). Figure 2(c) depicts the WGM spectra recorded from a smaller droplet of (18.00 ± 0.02) μm initial diameter. Optical coupling to such smaller ($d < 20$ μm) droplets proved to be rather difficult due to the small core size of the used single-mode fiber (8 μm). Figure 2(c) shows the 1st, 7th, and 14th spectra recorded from the droplet at times $t = 0$, 52.64, and 105.09 s, respectively. Here, the wavelength was scanned over a broader spectral range of 50 nm in order to reveal the relatively large FSR. Within the time interval of 105 s, the droplet diameter decreased significantly from (18 ± 0.02) μm to (12.7 ± 0.02) μm.

The dependence of the WGM Q-factor on the droplet size is shown in Fig. 3 for droplet diameters ranging between 12 and 54 μm. As shown in Fig. 3, the Q-factor has a tendency to increase with increasing droplet size. For the smallest studied droplet with initial diameter before dissolution $d = (18 \pm 0.02)$ μm (FSR = 29.3 nm), the measured FWHM was 4.5 nm, corresponding to a Q-factor of 5.2×10^2. At the other extreme, the narrowest measured FWHM was 0.08 nm for the droplet with $d = (45 \pm 0.02)$ μm (FSR = 11.75 nm), indicating a Q-factor of 1.8×10^4. Figure 3 also shows Q_{rad} values calculated for the parameter values used in our experiments using Eq. (5). Q_{rad} is obtained to be 8.1×10^3 and 5.5×10^7 for $d = 18$ μm and $d = 50$ μm droplets, respectively. We also performed absorption measurements on BB and calculated Q_{mat} using Eq. (2), as shown in the inset in Fig. 3. At the operating wavelength of $\lambda_0 = 1575$ nm, the calculated Q_{mat} for BB is 6.95×10^5. Hence, we conclude that for smaller droplets with $d \sim 18$ μm, the overall Q-factor is mainly determined by Q_{rad}, whereas absorptive and scattering losses become more dominant for larger droplets.

Losses due to absorption, scattering from particulate contaminants present in the droplet and host liquids, or perturbations in the size and shape of the droplet generally lead to shifts in the spectral position of WGMs and degradation of their Q-factor [29]. An illustration of this phenomenon is provided in Fig. 4 where fluctuating spectral shifts of WGMs to both blue and red ends of the spectrum are observed in consecutive spectra recorded from a single trapped droplet. Unlike the monotonic spectral drift observed in slowly dissolving droplets (see Fig. 2), spectral fluctuations shown in Fig. 4 are bi-directional, and their magnitude is significantly smaller.

In the first approximation, spectral shifts of WGM resonant wavelength due to the presence of a particulate contaminant in the mode volume inside the droplet cavity can be estimated from a simple geometric optics picture. Consider a contaminant particle with diameter D and refractive index n_c that is present within the WGM mode volume inside a droplet cavity of diameter d. Also, consider n_{eff} is the effective refractive index

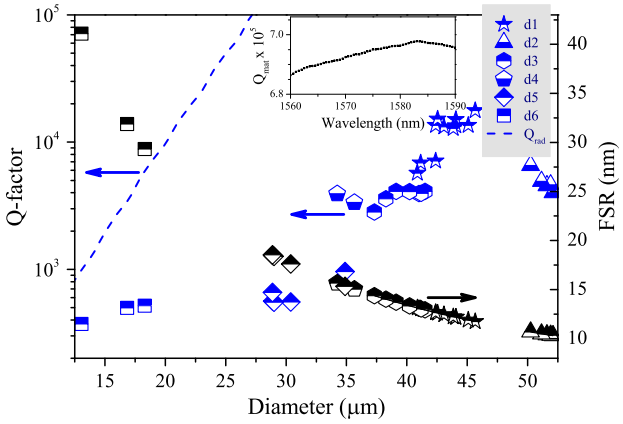

Fig. 3. Measured Q-factors of WGMs of BB droplets optically trapped in water with diameters varying from 12 to 54 μm. Symbols identify data points obtained from different droplets (d_1 to d_6). Dashed line shows Q_{rad} as a function of droplet diameter obtained using Eq. (5) after smoothing. Inset shows the measured spectral profile of Q_{mat} of BB in the wavelength range of interest.

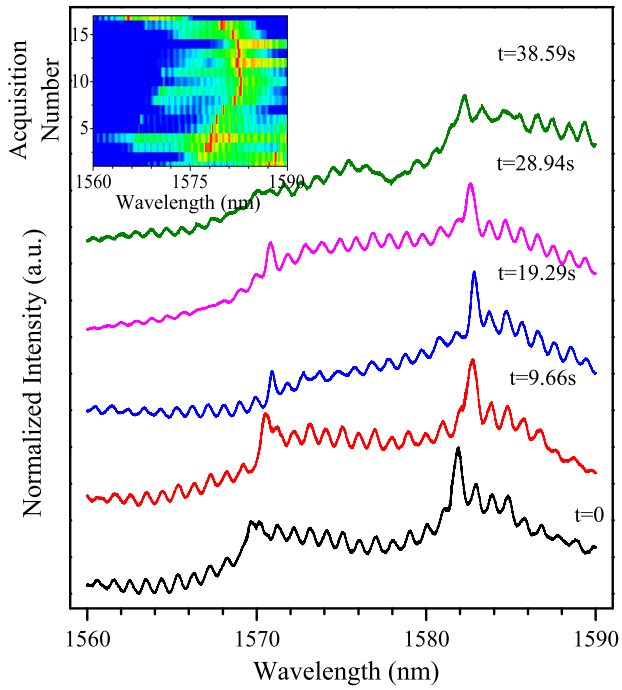

Fig. 4. Consecutive WGM spectra of a single 44 μm diameter BB droplet optically trapped in water, showing sensitivity to minute perturbations of the cavity and/or its environment. Inset shows the temporal evolution of 18 consecutive spectra.

of the WGM. On resonance, the optical path length of a WGM circulating in the vicinity of the cavity surface has to fulfill

$$(\pi d - D)n_{eff} + Dn_c = m\lambda, \tag{8}$$

where λ is the resonant wavelength of the perturbed cavity and m is the azimuthal mode order. Without the contaminant particle, the resonance condition for the same mode order is

$$\pi d n_{eff} = m\lambda_0. \tag{9}$$

Thus

$$\Delta\lambda \equiv (\lambda - \lambda_0) = \frac{D(n_c - n_{eff})}{\pi d n_{eff}}\lambda_0. \tag{10}$$

Equation (10) implies that for a contaminant particle with $n_c > n_{eff}$, the WGM resonant wavelength will be redshifted, whereas for $n_c < n_{eff}$, the WGM resonant wavelength will be blueshifted.

In the experiments summarized in Fig. 4, we observed fluctuating shifts of WGM resonant wavelength of $\Delta\lambda \approx \pm 1$ nm for the mean WGM wavelength $\lambda_0 = 1582$ nm and droplet diameter $d = 44$ μm. Assuming $n_{eff} \approx n_{int} = 1.568$, it follows from Eq. (10) that such WGM shifts could be caused by addition (blueshift) or removal (redshift) of microscopic water droplets ($n_c = 1.334$) of diameter $D \approx 0.6$ μm to the mode volume. Contaminant particles in this size range which were likely generated during mechanical agitation of the emulsion were indeed observed inside BB droplet cavities in some experiments. Strictly speaking, in our situation, we operate outside the limits of validity of geometric optics treatment; nevertheless, this simple approach still captures the essence

of WGM wavelength shifts due to perturbations of the WGM field by a particulate contaminant with a RI different from that of the cavity.

5. CONCLUSION

We have demonstrated a new and simple approach for stable and efficient free-space optical coupling to WGMs of droplet resonators immobilized and positioned in an immiscible host liquid by using optical tweezers integrated with a microfluidic channel. Elastically scattered light from optically trapped emulsion droplets has been analyzed and Q-factors as high as 1.8×10^4 have been measured for droplets with a diameter of 45 μm. We have also observed the dependence of the average Q-factor of the cavity WGMs on the droplet size for diameters between 18 and 50 μm. Prolonged monitoring of WGM spectra of an individual optically trapped droplet revealed fluctuations in WGM spectral positions, thus hinting at the possibility of sensing minute perturbations of the cavity and/or its environment in biological and chemical analysis. Further investigation of optical properties of droplet-based microcavities can lead to the development of useful intracavity sensing schemes for monitoring biochemical processes occurring inside the droplets, a powerful tool for a lab-on-a-chip.

Funding. Türkiye Bilimsel ve Teknolojik Araştırma Kurumu (TÜBİTAK) (114C030, 114F253).

Acknowledgment. We thank M. Aas for help with incorporating optical fibers into microfluidic chips.

REFERENCES

1. R. E. Benner, P. W. Barber, J. F. Owen, and R. K. Chang, "Observation of structure resonances in the fluorescence spectra from microspheres," Phys. Rev. Lett. **44**, 475–478 (1980).
2. A. Ashkin and J. M. Dziedzic, "Observation of optical resonances of dielectric spheres by light scattering," Appl. Opt. **20**, 1803–1814 (1981).
3. A. Serpengüzel, G. Griffel, and S. Arnold, "Excitation of resonances of microspheres on an optical fiber," Opt. Lett. **20**, 654–656 (1995).
4. C. G. B. Garrett, W. Kaiser, and W. L. Bond, "Stimulated emission into optical whispering gallery modes of spheres," Phys. Rev. **124**, 1807–1809 (1961).
5. P. Michler, A. Kiraz, C. Becher, L. Zhang, E. Hu, A. Imamoglu, W. V. Schoenfeld, and P. M. Petroff, "Quantum dot lasers using high-Q microdisk cavities," Phys. Status Solidi B **224**, 797–801 (2001).
6. A. Kiraz, A. Sennaroglu, S. Doganay, M. A. Dundar, A. Kurt, H. Kalaycioglu, and A. L. Demirel, "Lasing from single, stationary, dye-doped glycerol/water microdroplets located on a superhydrophobic surface," Opt. Commun. **276**, 145–148 (2007).
7. V. Sandoghdar, F. Treussart, J. Hare, V. Lefevre-Seguin, J.-M. Raimond, and S. Haroche, "Very low threshold whispering-gallery-mode microsphere laser," Phys. Rev. A **54**, R1777–R1780 (1996).
8. Y. K. S. Suzuki, Y. Hatakeyama, and S. T. Chu, "Precise control of wavelength channel spacing of microring resonator add-drop filter array," J. Lightwave Technol. **20**, 745–750 (2002).
9. C. Z. P. Rabiei, W. H. Steier, and L. R. Dalton, "Polymer micro-ring filters and modulators," J. Lightwave Technol. **20**, 1968–1975 (2002).
10. M. R. Foreman, J. D. Swaim, and F. Vollmer, "Whispering gallery mode sensors," Adv. Opt. Photon. **7**, 168–240 (2015).
11. A. Jonáš, Y. Karadag, M. Mestre, and A. Kiraz, "Probing of ultrahigh optical Q-factors of individual liquid microdroplets on superhydrophobic surfaces using tapered optical fiber waveguides," J. Opt. Soc. Am. B **29**, 3240–3247 (2012).
12. D. W. Vernooy, V. S. Ilchenko, H. Mabuchi, E. W. Streed, and H. J. Kimble, "High-Q measurements of fused-silica microspheres in the near infrared," Opt. Lett. **23**, 247–249 (1998).
13. D. McGloin, D. R. Burnham, M. D. Summers, D. Rudd, N. Dewar, and S. Anand, "Optical manipulation of airborne particles: techniques and applications," Faraday Discuss. **137**, 335–350 (2008).
14. Y. Karadag, M. Aas, A. Jonáš, S. Anand, D. McGloin, and A. Kiraz, "Dye lasing in optically manipulated liquid aerosols," Opt. Lett. **38**, 1669–1671 (2013).
15. A. M. Armani and K. Vahala, "Heavy water detection using ultra-high-Q microcavities," Opt. Lett. **31**, 1896–1898 (2006).
16. L. Shao, X.-F. Jiang, X.-C. Yu, B.-B. Li, W. R. Clements, F. Vollmer, W. Wang, Y.-F. Xiao, and Q. Gong, "Detection of single nanoparticles and lentiviruses using microcavity resonance broadening," Adv. Mater. **25**, 5616–5620 (2013).
17. S. Avino, A. Krause, R. Zullo, A. Giorgini, P. Malara, P. D. Natale, H. P. Loock, and G. Gagliardi, "Direct sensing in liquids using whispering-gallery-mode droplet resonators," Adv. Opt. Mater. **2**, 1155–1159 (2014).
18. S. Kaminski, L. L. Martin, and T. Carmon, "Tweezers controlled resonator," Opt. Express **23**, 28914–28919 (2015).
19. M. L. Gorodetsky, A. A. Savchenkov, and V. S. Ilchenko, "Ultimate Q of optical microsphere resonators," Opt. Lett. **21**, 453–455 (1996).
20. M. L. Gorodetsky and V. S. Ilchenko, "Optical microsphere resonators: optimal coupling to high-Q whispering-gallery modes," J. Opt. Soc. Am. B **16**, 147–154 (1999).
21. H. M. Lai, P. T. Leung, and K. Young, "Limitations on the photon storage lifetime in electromagnetic resonances of highly transparent microdroplets," Phys. Rev. A **41**, 5199–5204 (1990).
22. M. Aas, A. Jonáš, A. Kiraz, O. Brzobohatý, J. Ježek, Z. Pilát, and P. Zemánek, "Spectral tuning of lasing emission from optofluidic droplet microlasers using optical stretching," Opt. Express **21**, 21380–21394 (2013).
23. L. F. Phillips, "A geometrical explanation for the enhanced small-scale roughness of a liquid surface," J. Phys. Chem. B **108**, 1986–1991 (2004).
24. G. C. Righini, Y. Dumeige, P. Feron, M. Ferrari, G. N. Conti, D. Ristic, and S. Soria, "Whispering gallery mode microresonators: fundamentals and applications," Riv. Nuovo Cimento Soc. Ital. Fis. **34**, 435–488 (2011).
25. I. S. Grudinin, V. S. Ilchenko, and L. Maleki, "Ultrahigh optical Q factors of crystalline resonators in the linear regime," Phys. Rev. A **74**, 063806 (2006).
26. H. Hulst and H. van de Hulst, *Light Scattering by Small Particles*, Dover Books on Physics (Dover Publications, 1957).
27. P. Chýlek, J. T. Kiehl, and M. K. W. Ko, "Optical levitation and partial-wave resonances," Phys. Rev. A **18**, 2229–2233 (1978).
28. E. J. G. Peterman, F. Gittes, and C. F. Schmidt, "Laser-induced heating in optical trap," Biophys. J. **84**, 1308–1316 (2003).
29. A. Jonáš, M. Aas, Y. Karadag, S. Manioglu, S. Anand, D. McGloin, H. Bayraktar, and A. Kiraz, "In vitro and in vivo biolasing of fluorescent proteins suspended in liquid microdroplet cavities," Lab Chip **14**, 3093–3100 (2014).